Available online at www.sciencedirect.com
SCIENCE DIRECT®
Surface Science 530 (2003) 181–194
SURFACE SCIENCE
www.elsevier.com/locate/susc

Scanning probe microscopy characterization of gold-chemisorbed poplar plastocyanin mutants

L. Andolfi [a,b], B. Bonanni [a], G.W. Canters [b], M.Ph. Verbeet [b], S. Cannistraro [a,*]

[a] *Unita INFM, Dipartimento di Scienze Ambientali, Università della Tuscia, Largo dell'Universita, I-01100 Viterbo, Italy*
[b] *Leiden Institute of Chemistry, Gorlaeus Laboratoria, Leiden University, The Netherlands*

Received 14 February 2003; accepted for publication 7 March 2003

Abstract

Two poplar plastocyanin mutants adsorbed onto gold electrodes have been characterized at single molecule level by scanning probe microscopy. Immobilization of the two redox metalloprotein mutants on Au(1 1 1) surface was achieved by either a disulphide bridge (PCSS) or a single thiol (PCSH), both the anchoring groups having been introduced by site-directed mutagenesis. Scanning tunneling microscopy (STM) and atomic force microscopy (AFM) analysis gives evidence of a stable and robust binding of both mutants to gold. The lateral dimensions, as estimated by STM, and the height above the gold substrate, as evaluated by AFM, of the two mutants well agree with crystallographic sizes. A narrower height distribution is observed for PCSS compared to PCSH, corresponding to a more homogeneous orientation of the former mutant adsorbed onto gold. Major differences between the mutants are observed by electrochemical STM. In particular, the image contrast of adsorbed PCSS is affected by tuning the external electrochemical potential to the redox levels of the mutant, consistent with some involvement of copper active site in the tunneling process. On the contrary, no contrast variation is observed in electrochemical STM of adsorbed PCSH. Moreover, scanning tunneling spectroscopy experiments reveal asymmetric *I–V* characteristics for single PCSS proteins, reminiscent of a rectifying-like behaviour, whereas an almost symmetric *I–V* relation is observed for PCSH.

Keywords: Biological molecules – proteins; Scanning tunneling microscopy; Scanning tunneling spectroscopies; Atomic force microscopy; Self-assembly

1. Introduction

The characterization of redox metalloproteins chemisorbed onto metal electrodes is gaining great interest in the progressing interdisciplinary research field of bioelectronics that involves the integration of biomaterials with electronic transducers, such as electrodes, field-effect-transistors and piezoelectric crystals [1,2]. Copper proteins and their localized redox centres, which are responsible for the electron transfer (ET) function, have been extensively characterised structurally in recent years [3]. The ET mechanism of such proteins is very efficient. In general they are part of ET chains where the conduction through the biomolecule occurs at the level of the single electron [4,5]. This feature renders copper proteins promising

* Corresponding author. Tel.: +39-0761-357136; fax: +39-0761-357179.
E-mail address: cannistr@unitus.it (S. Cannistraro).

0039-6028/03/$ - see front matter
doi:10.1016/S0039-6028(03)00443-6

candidate for the construction of low dissipation, highly sensitive hybrid mono-molecular devices. The ability to obtain functional and oriented metalloprotein adlayers is an important route toward this goal. Furthermore, covalent bonding of a molecule to a conductor is a key requirement for efficient conduction through a single molecule towards the electrode. In this perspective, the high affinity of disulphides and thiols for gold electrodes has been amply investigated [6]. Experimental and theoretical studies showed that dissociative reduction of a disulphide with subsequent formation of strongly bound thiolates can be achieved [7,8], whereas the binding of thiolates resulting from S–H bond cleavage in thiols is accompanied by the development of molecular hydrogen [8]. Native disulphide and thiols have been estensively exploited to achieve protein–metal adsorption [9–13].

Thus copper proteins fulfill the basic requirements for integration in nanobiodevices thanks also to the possibility of tuning their redox potential. In the present work, we focus on poplar plastocyanin (PC). PC is a small blue copper protein (10.5 KDa) acting as an electron carrier between cytochrome *f* and P700 in the photosynthetic ET chain. Its structural features include a distorted tetrahedral copper site at one end of an eight-stranded antiparallel β barrel [14]. The tetrahedral geometry of the copper site facilitates the ET that results from a transition from the oxidized to the reduced state with a characteristic redox potential [14]. To make poplar PC suitable for stable and specific self-assembly onto gold, we designed two mutants bearing anchoring groups that carry sulphur atoms. In the first mutant (PCSS), a disulphide bridge was inserted within the protein, while in the second one (PCSH) a residue tail, containing among others a cysteine, was added as C-terminal extension. Both groups (S–S and S–H) are located in a region of the protein opposite to the copper active site and easily available for chemisorption onto a gold electrode, as schematically represented in Fig. 1. By the introduction of the anchoring groups, it should be possible to both create well-defined molecular adlayers of high stability and, more importantly, to control the electronic coupling between the metalloprotein (including the copper containing active site) and the underlying gold electrode surface. Due to the diverse locations of the anchoring groups we expect different effects on both topographical and conductive properties of adsorbed PC mutants when immobilizing via either the SH and the S–S moiety.

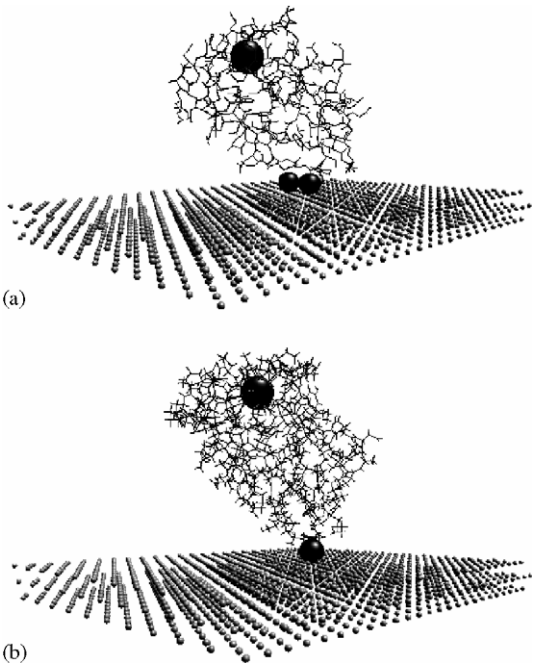

Fig. 1. Visual molecular dynamics graphic representation showing the two plastocyanin mutants immobilized via the S–S (a) or S–H group (b) onto an Au(1 1 1) substrate. The copper atom is indicated by the sphere at the top, the sulfur atoms are indicated by smaller spheres at the bottom. Coordinates for PCSS are from X-ray crystallography [29]. The three dimensional structure of PCSH is obtained from the PDB file of wild type plastocyanin (Brookhaven Protein Database) after adding the three residue tail at the C-terminal position (see Section 2) by Swiss PDB Viewer (SPDBV).

To compare the two linkages and to investigate possible influences on the conformational and conducting properties of the immobilised proteins at the single molecule level, we focus on the characterisation of the two immobilised mutants by scanning probe microscopy (SPM). Indeed SPM, when compared to conventional techniques to study adsorption of protein monolayers [15–18], allows the characterisation of adsorbed proteins at

concentrations below monolayer coverage [19–21], thus minimizing protein–protein interaction. In particular, in the present work the combination of scanning tunneling microscopy (STM) and atomic force microscopy (AFM) provides complementary information on the electronic properties and morphology of individual proteins, under physiological and ambient conditions. STM measures the tunneling current and represents a powerful tool to investigate electronic properties of single molecules [22] with submolecular resolution. Scanning tunneling spectroscopy (STS) can be performed to acquire I–V data by selectively positioning the tip over a single protein [23]. AFM provides reliable information about molecule height and orientation above the substrate [19,24,25].

Here we present an extensive characterisation of PCSS and PCSH monolayers, in which a single molecule has a lateral size (evaluated by STM) and a vertical dimension (measured by AFM) in close agreement with the crystallographic data, although PCSS molecules present a narrower height distribution above the substrate. Electrochemical STM indicates a possible contribution of protein redox levels in the image contrast formation for PCSS; such behaviour has not observed for PCSH. Besides, single molecule STS shows a rectifying-like behaviour for PCSS, which is not detected in the PCSH molecule.

2. Materials and methods

2.1. Mutagenesis, expression and purification

Design, expression and purification of PCSS were carried out as reported previously [26]. PCSH was designed and expressed as follows: for PCR-mutagenesis the *pET-3a* plasmid [27], containing the wild type poplar plastocyanin gene was used as a template. A mutagenic primer coding for a C-terminal extension was synthesised. As a result a sequence encoding three extra C-terminal residues [Thr–Cys–Gly] was incorporated in the gene. Sequence analysis confirmed the mutation. The expression vector with the mutated gene was constructed by using a combination of restriction sites resulting in a PCSH expressing *pET-3* plasmid [26]. The PCSH mutant was over-expressed in the cytoplasm of *E. coli HMS174* (DE3) and grown at 37 °C in $2\times$ YT medium supplemented with 100 μg/ml of carbenicillin and 0.1 mM copper citrate. Protein expression was induced by addition of 0.2 mM IPTG. The PCSH mutant variant was isolated from bacteria by the freeze/thaw method [28]. Subsequently, the protein was purified by anion-exchange chromatography (DEAE Sefharose fast flow) and Superdex G-75 size exclusion column chromatography in a Pharmacia FPLC setup [26]. The N-terminal sequence and the mass (by electron spray mass spectroscopy) were determined at the Protein sequencing facility, LUMC, Leiden. In the mass spectra a dominant form, corresponding to a PCSH glutathione extension, was revealed.

The protein integrity and the copper site properties for PCSS was assessed by extensive spectroscopic and structural characterization as described elsewhere [26,29]. Similar spectroscopic techniques have been used to characterise PCSH showing protein integrity and properties of the copper site closely resembling those of the wild type protein. Optical spectroscopy on both mutants provided a value of 1.1 for the absorbance ratio A_{280}/A_{597}, indicating similar high purity characteristics for the two preparations [26]. The redox functionality of the PCSS and PCSH upon immobilisation onto a gold electrode was assessed by preliminary cyclic voltammetry experiments [30].

2.2. STM measurements

STM images were acquired by a Picoscan system (Molecular Imaging Co.) equipped with a Picostat (Molecular Imaging Co.) bipotentiostat. A 10-μm scanner with a final preamplifier sensitivity of 1 nA/V was used for STM measurements. Images were acquired both in air and in buffer solution in constant current mode, using electrochemically etched Pt/Ir tips purchased from Molecular Imaging. Gold substrates deposited on mica (Molecular Imaging) were flame-annealed to obtain recrystallized terraces. STM analysis (not shown here) confirmed the presence of atomically flat (1 1 1) terraces, a few hundreds of nanometers in size. The measuring cell for electrochemical

STM consisted of a Teflon™ ring pressed over the Au(1 1 1) substrate operating as a working electrode. A 0.5 mm Pt wire was used as counter electrode and a 0.5 mm Ag wire as a quasi-reference electrode (AgQref). The AgQref potential was measured vs saturated calomel electrode (SCE). In what follows, the potential is always referred to SCE.

Current–voltage curves were obtained by setting the gap at a tunneling current of 50 pA and V_{bias} of 0.180 V; disengaging the feedback, the tunneling current was monitored as the substrate potential is swept over ±1 V, and every single sweep was collected in 0.01 s.

Protein adsorption onto gold was accomplished by incubating the Au(1 1 1) annealed substrates with a 20 μM protein solution (20 mM sodium phosphate, pH 6.0), at 4 °C for 30 min. After incubation, samples were gently rinsed with ultrapure water (resistivity 18.2 ΩM cm), blown dry with a soft jet of pure nitrogen, and immediately imaged for scanning in ambient conditions, or immersed in buffer solution for fluid imaging.

2.3. AFM measurements

Topographic images of the surface were taken with a Nanoscope IIIa/Multimode scanning probe microscope (Digital Instruments) equipped with a 12-μm scanner (E scannner) operating in tapping mode (TM). In this configuration the tip is kept oscillating at its resonant frequency; the reduction in oscillation amplitude (due to tip-surface interaction) is used to identify and measure surface features. In TM the tip just barely "hits" or taps the sample, drastically reducing frictional forces as compared to contact-mode AFM. As a result, tip induced damage over the molecules is minimal and reliable data about the molecular height distribution over the gold substrate can be obtained.

Oxide-sharpened silicon nitride probes (Digital Instruments), 100 or 200 μm long and with nominal spring constant of 0.15 and 0.57 N/m respectively, were used. All protein imaging was performed in buffer solution using the fluid cell without the O-ring seal, in order to minimize the lateral drift that is often caused by O-ring pressure over the sample. Before engaging, scan size and offsets were set to zero to minimize sample deformation and contamination of the tip. Free oscillation of the cantilever was set to have a root-mean-square amplitude corresponding to ~1.5 V. Before scanning the sample, the set point was adjusted to minimal forces.

The quality of the annealed gold substrates was controlled by contact mode AFM measurements in air. High quality Au(1 1 1) recrystallized terraces show a roughness of about 0.1 nm. The substrates were incubated at 4 °C with 7 μM protein solution in 20 mM sodium phosphate buffer, pH 6.0, for periods ranging from 30 min to 12 h. After incubation, samples were gently rinsed with ultrapure water to remove weakly adsorbed proteins and readily covered with 35 μl of buffer solution for immediate fluid imaging. As a control, Au(1 1 1) substrates were treated in similar way but without the addition of proteins. They were scanned under identical conditions to ensure that no spurious images would be obtained.

3. Results and discussion

3.1. STM characterization

Adsorbed PCSS and PCSH molecules have been imaged by STM under buffer solution, as shown in Fig. 2(a) and (b) respectively. Self-assembled proteins appear to be stable and to give reproducible images during repetitive scans, confirming a robust binding of the proteins on Au(1 1 1). In contrast, analogous STM experiments performed on adsorbed wild type PC revealed protein mobility over the substrate upon repeating scans, which indicates that no stable binding occurs for PC in the absence of S–S or S–H groups (data not shown). In Fig. 2(a), individual PCSS molecules are clearly discerned, whose average lateral dimension, as evaluated by cross section, is 4.2 ± 0.4 nm, close to that obtained from X-ray crystallography [29]. In the case of PCSH (Fig. 2(b)) molecules with a shape matching those observed for PCSS were revealed on the gold surface. The lateral size of such molecules, as estimated by cross section, is 4.5 ± 0.4 nm, comparable to that obtained for PCSS in the range of experimental error. Even if

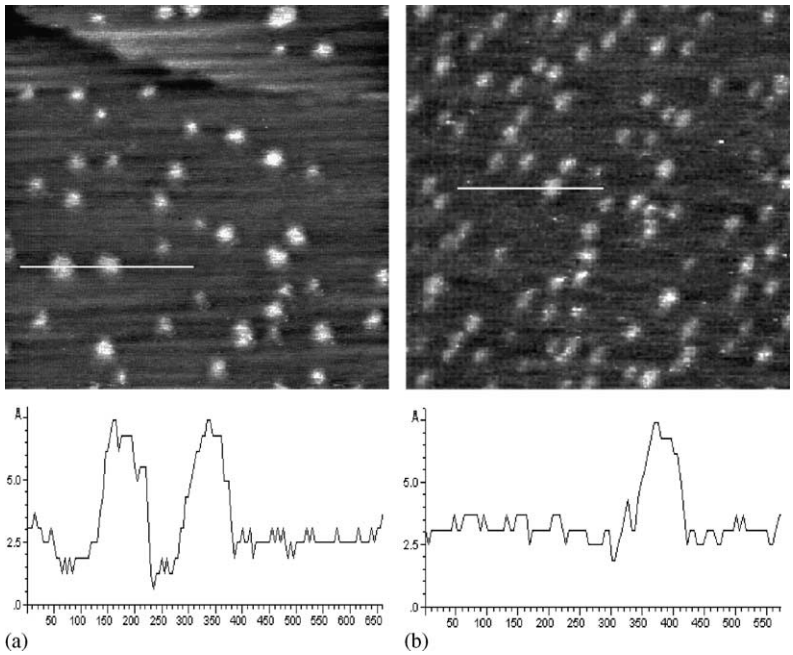

Fig. 2. Constant current STM images of PCSS (a) and PCSH (b) molecules on Au(1 1 1) in 50 mM ammonium acetate, pH 4.6. Scan area: 130×130 nm^2. Tunneling current 50 pA, bias voltage 0.180 V (tip positive), scan rate 4 Hz. Representative cross section profiles for adsorbed molecules are shown in lower panels; molecular height and lateral size can be evaluated from maximum vertical size and from full width half maximum, respectively.

the X-ray structure for PCSH in not available, lateral sizes of immobilised proteins well compare to those evaluated from the three-dimensional model structure represented in Fig. 1, and obtained as described in the corresponding caption.

The estimated vertical size of PCSS and PCSH, as shown in the cross section of Fig. 2, appears to be in the range of 0.5–0.7 nm. Comparing such dimensions with crystallographic data [29] we observe that the vertical size of the molecules above the substrate is significantly smaller than the value expected for PC anchored to gold via the disulphide bridge (PCSS) or via the single thiol (PCSH). With reference to graphical representations of the PC mutants with the anchoring groups assumed to be 'face down' for covalent binding to gold (see Fig. 1), one expects a vertical size of about 3 nm. Indeed, the considerable height reduction of biological materials in STM imaging was already observed in numerous previous investigations [10,13,31–33] and only in few cases the physical height of the biomolecules has been reported [34,35]. Such a discrepancy is still a controversial aspect in the interpretation of STM images. Although a number of groups have reported successful STM imaging of biomolecules, the origin of the contrast in protein molecules is not understood. Proteins are a class of insulators/quasi conductors and the concept of vacuum tunneling cannot explain the tunneling through a molecular medium. In some reports it has been proposed that the STM contrast of adsorbates on metallic surface arises from modification of metallic states at the Fermi energy caused by the interaction of the molecule with the metal surface [22]. Other STM reports pointed out that the ionic conductivity through a surface water film plays an important role in tunneling between the STM tips and the sample surface [36]. For high vacuum STM of biological molecules an electric field-induced mechanism for conduction of electrons through the molecule was suggested [34]. In the case of metalloproteins, the redox centre (the copper containing active site for PC) was proposed

to mediate the tunneling current [9,13,37]. This has been interpreted in the framework of two theoretical models. One model takes into account the effect of the coupling between adsorbate redox levels and the substrate Fermi level. In this model [37] electrons tunnel from tip to substrate (or vice-versa) by a resonant tunneling process through the molecular unoccupied states (oxidised states) when they are brought to align with the substrate or tip Fermi level. In a second model a strong coupling of molecular electronic states with the nuclear fluctuations is considered. In this case the ETs to the protein and reduces the copper site, which begins to relax vibrationally; this relaxation allows the molecule to transfer the electron to the other electrode and to return to its oxidised state [9,38]. Even if the physical mechanism governing the STM process through a redox molecule has not been fully established, it is commonly accepted that STM images are a complex convolution of topographic and electronic contributions and the height of biomolecules as measured by STM may deviate significantly from the purely topographic one.

With the aim to investigate the ET capabilities of the adsorbed mutants, as well as the role of the copper atom in the tunneling mechanism, we have performed STM imaging under electrochemical control. This condition offers the possibility to tune the electrochemical potential of the working electrodes to the protein redox midpoint potential [9,11,13], allowing the investigation of image contrast in relation to the ET properties of the molecule. By using a bipotentiostat, the electrochemical potential of the two working electrodes (substrate and tip) was tuned in a wide range around the redox midpoint potential (+106 mV, [26]). In Fig. 3 we show a sequence of in situ STM images of PCSS adsorbed on Au(1 1 1) for three of the several substrate electrochemical potentials investigated, ranging between −222 and +28 mV vs SCE. The molecular features are clearly visible for substrate potentials close to the midpoint potential (Fig. 3(a)), the image contrast is weaker when the potential is far from this value (Fig. 3(b)) and it is recovered once the initial potential is re-established (Fig. 3(c)). This effect is also reflected in slight changes of height in the cross sections. Such results seem to be consistent with previous studies on azurin in which a full bleaching was observed [13]. They support, as already predicted by theoretical models [37,38], that the copper site represents a preferential way for the tunneling process through the protein, once its redox levels are

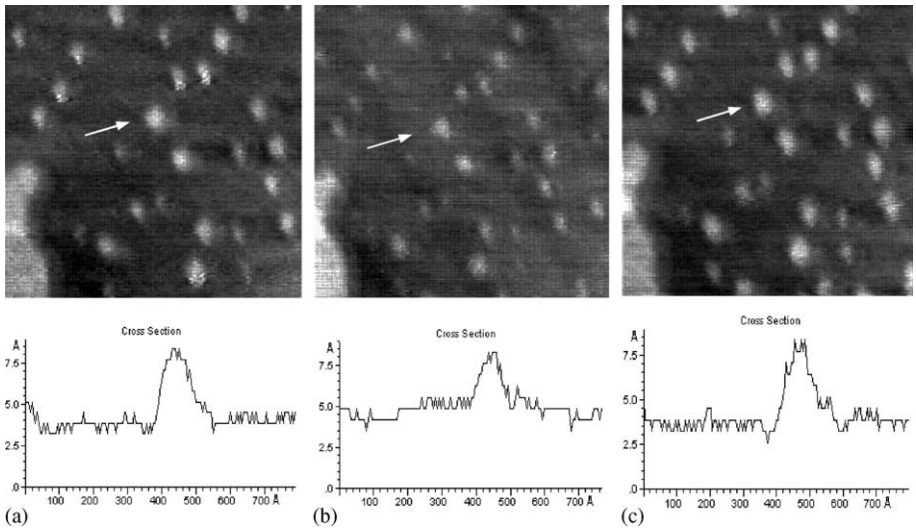

Fig. 3. STM imaging under electrochemical control in constant current mode of PCSS molecules in 50 mM ammonium acetate, pH 4.6. Scan area: 120×120 nm^2. Tunneling current 50 pA; V_{bias} 0.180 V (tip positive), scan rate 4 Hz. Substrate potential is +28 mV vs SCE (a), −222 mV vs SCE (b), +28 mV vs SCE (c). Single molecule cross section profiles are shown in the lower panel.

properly aligned with the substrate and tip Fermi levels. These findings are also consistent with a recent voltammetric analysis, which shows that the plastocyanin mutant adsorbed on a gold electrode preserves its redox functionality [30].

Similar STM experiments under electrochemical control were performed for the PCSH mutant. In Fig. 4(a)–(c) a sequence of electrochemical STM images is shown for substrate electrochemical potentials ranging from −222 to +28 mV vs SCE. No relevant contrast variation is observed upon sweeping substrate potential, as is also evident from the unchanged height in the cross sections. On the other hand, the redox functionality of adsorbed PCSH seems to be retained upon preliminary cyclic voltammetry experiments (data not shown). Therefore, we can hypothesize that the higher protein flexibility resulting from immobilisation via external S–H may result in an unfavourable alignment of molecular redox levels with tip and substrate Fermi levels [9,13,39].

Taking also into account the different electrochemical STM features of the two mutants, immobilised PCSS and PCSH have been further investigated by STS experiments under ambient conditions, in order to obtain additional information about their electronic properties.

Before recording biomolecule current–voltage curves, preliminary STM imaging of both mutants adsorbed onto gold has been performed in ambient conditions. Representative STM images for PCSS and PCSH are shown in Fig. 5(a) and (b) respectively. Even in ambient conditions, images were stable and reproducible revealing globular structures of lateral size comparable with the crystallographic one and vertical dimensions smaller than the expected values, as evident from a cross section analysis. For STS ambient experiments, the tip has been positioned over the central brighter area of the molecules. In Fig. 6 consecutive I–V curves (each averaged over 10 sweeps) acquired for a single PCSS molecule are shown. We observe a progressive decrease in the current response of PCSS. The conductivity measured in the first curve is not recovered after repeated scans, although the I–V curves preserve a characteristic asymmetry, when comparing data for positive and negative bias. Changes in conductive response after consecutive I–V measurements are also reflected in STM imaging. Fig. 7 shows a sequence of high-resolution STM images of single molecules, each image was acquired before the I–V scans reported in Fig. 6. A progressive decrease of STM contrast is clearly observed: the bright central area of the

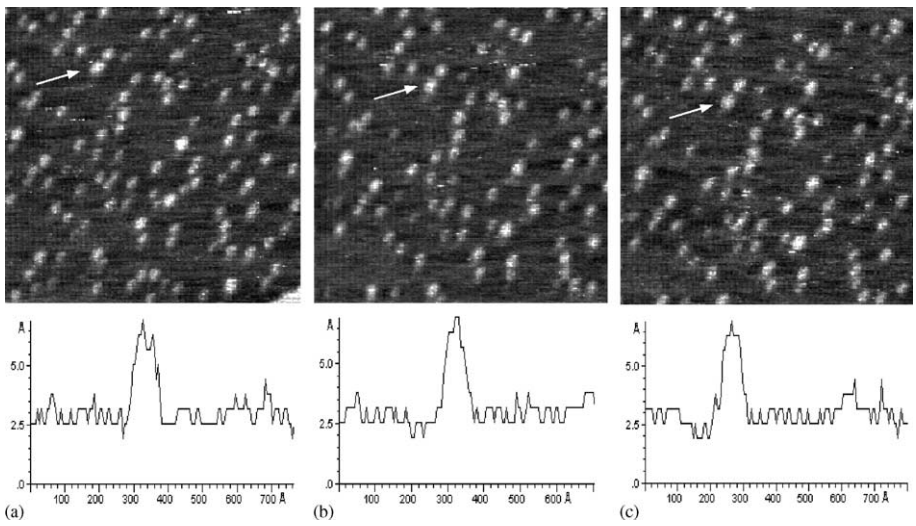

Fig. 4. STM imaging under electrochemical control in constant current mode of PCSH molecules in 50 mM ammonium acetate, pH 4.6. Scan area: 140×140 nm^2. Tunneling current 50 pA, V_{bias} 0.180 V (tip positive), scan rate 4 Hz. Substrate potential is +28 mV vs SCE (a), −222 mV vs SCE (b), +28 mV vs SCE (c). Single molecule cross section profiles are shown in the lower panel.

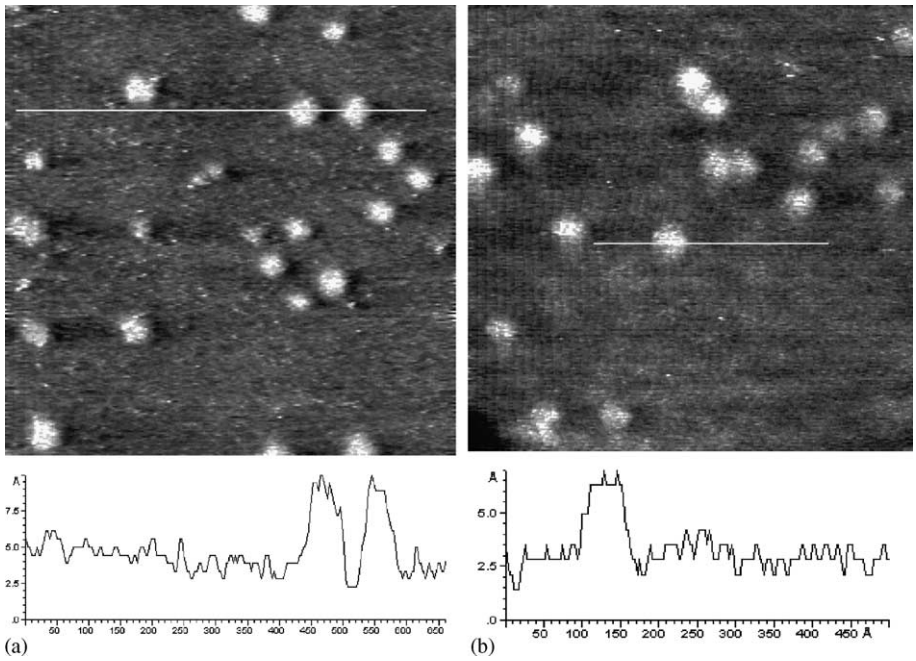

Fig. 5. STM images of PCSS (a) and PCSH (b) in ambient conditions. Scan area: 70×70 nm^2 (a) and 73×73 nm^2 (b). Tunneling current 50 pA, V_{bias} 0.180 V (tip positive), scan rate 4 Hz. Cross section profiles through the molecules are shown in the lower panels.

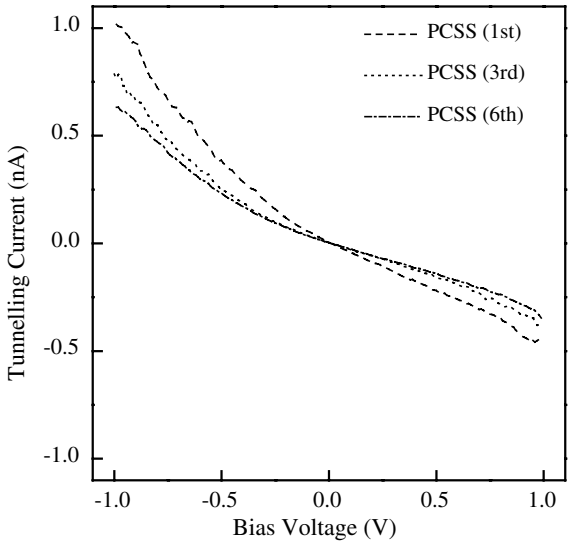

Fig. 6. Consecutive I–V curves recorded on a single PCSS molecule in ambient conditions. The engage tunneling current and bias voltage are 50 pA and 0.180 V (tip positive), respectively. Each curve is obtained as the average over 10 I–V sweeps.

molecule disappears after the first I–V scan, and the initial height of the spot in the STM image is not recovered.

To avoid consecutive sweeping on a single molecule, which is likely to produce unstable I–V results, the conducting properties of plastocyanin mutants have been further investigated by STS experiments performed over several distinct adsorbed molecules. The I–V curve obtained from I–V measurements over 22 different PCSS molecules (the I–V curve for each molecule being averaged over 10 sweeps, with an overall number of 220 sweeps) is shown in Fig. 8(a), together with the I–V data for Au(1 1 1). The slight asymmetry observed for gold finds its explanation in the atomic structure of the tip apex [40]. In contrast to this, PCSS single molecules exhibit a clear pronounced and reproducible asymmetric I–V relation. This asymmetry, reminiscent of a rectifying-like behaviour, has already been reported in previous STS experiments on electroactive molecules, and interpreted in terms of a redox mediated tunneling process [22,23,41–43]. Other models, accounting

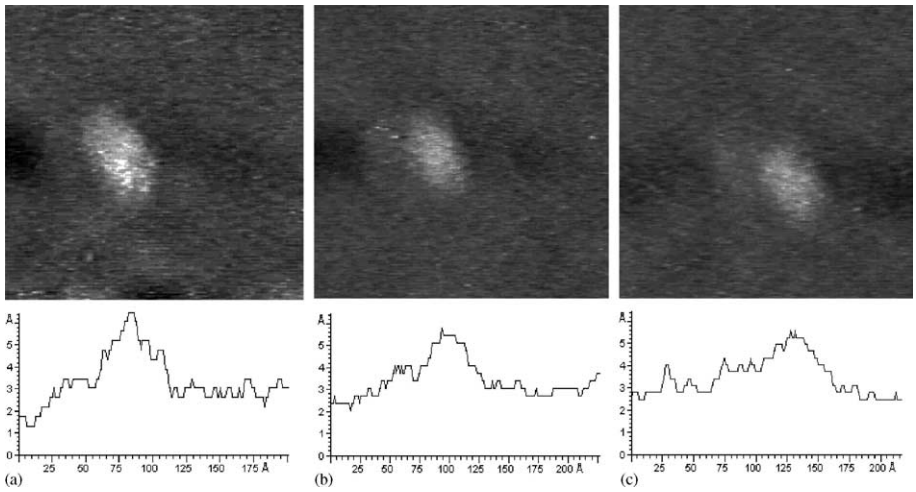

Fig. 7. High-resolution STM images of a single PCSS molecule acquired before first (a) third (b) and last I–V curve (c) shown in Fig. 6. Scan area: 20×20 nm^2. Current set point and bias voltage are 50 pA and 0.180 V (tip positive), respectively. Molecule cross section profiles are shown in the lower panel.

for molecular rectification, have been developed, as for the metal–insulator–metal junction with an organic molecule, containing a donor–acceptor pair, placed between the metal electrodes [44,45]. In more recent reports it was shown that a rectifying behaviour for metal–insulator–metal junction can be obtained even when using molecules which do not contain donor-acceptor pairs. In some cases the rectification was attributed to the presence of a single electron acceptor asymmetrically placed in a metal–insulator–metal junction [46], or to conformational changes driven by the external electric field [47], or even to Schottky barrier effects [48]. Therefore, it is clear that molecular rectification is not an unambiguously resolved process and its mechanism is currently under investigation. However, in connection with the theories discussed above [37,38], a possible explanation of the STS results for the PCSS mutant is that the copper site immersed in the protein matrix has a central role in generating the $I(V)$ asymmetry. Such a hypothesis is supported also by the fact that in a detailed STS study on self-assembled copper proteins [49] a clear $I(V)$ asymmetry is observed. In this case the $\mathrm{d}I/\mathrm{d}V$ vs V curve, which is a direct measure of the local density of the states of the sample, can be fitted with a gaussian curve, whose maximum peak position seems to be related to the redox potential of the copper proteins [49]. These results suggest that a spatial coupling asymmetry between the copper density of states and the electrode Fermi energy is likely to exist. The asymmetric behaviour we observe in PCSS molecules confirms, even in ambient conditions, a possible involvement of copper redox site in the tunneling mechanism.

For comparison, STS experiments have been performed also on several distinct PCSH molecules. In Fig. 8(b) the I–V curve averaged over 50 different PCSH molecules (with an overall number of 500 sweeps) is plotted together with data for gold. Although PCSH in STM images appears to have features similar to PCSS (see Fig. 5), the two mutants show a clearly different behaviour in STS. The I–V curves for PCSH were observed to be mostly symmetric when comparing data for positive and negative bias. In connection to what was observed in the electrochemical STM, the measured I–V relation for PCSH molecules seems to be related to an unfavourable interplay of the redox levels with the Fermi levels of substrate and tip.

However, it is worth noticing that in STM/STS experiments the stress applied by the tip over the

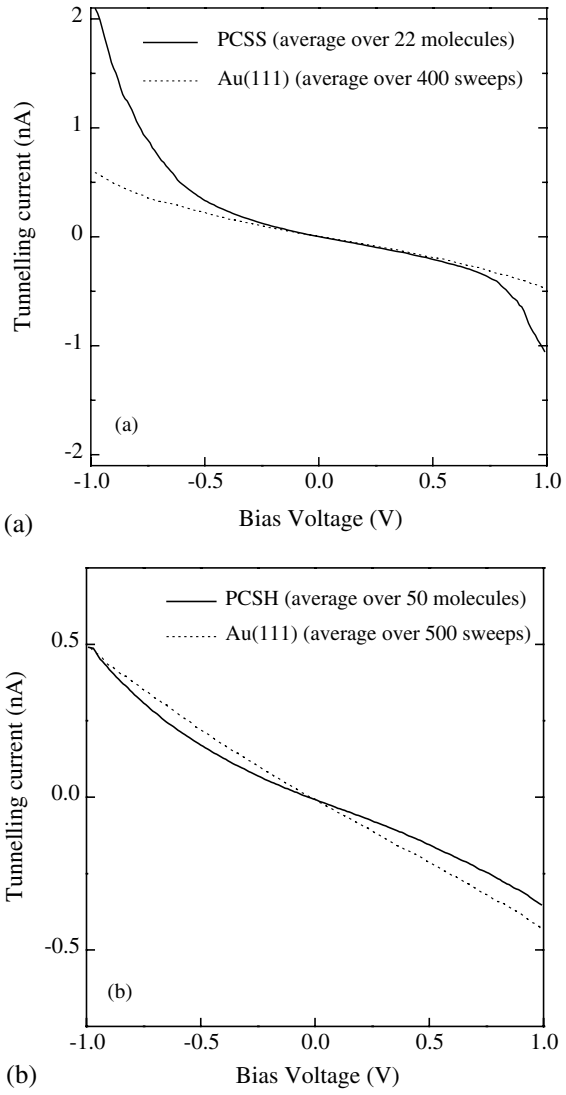

Fig. 8. (a) *I–V* curves recorded in ambient conditions on 22 different PCSS molecules (data for each molecule are averaged over 10 *I–V* sweeps) and on Au(1 1 1); (b) *I–V* curves recorded in ambient conditions on 50 different PCSH molecules (10 sweeps are averaged for each molecule) and on Au(1 1 1). The engage tunneling current and bias voltage are 50 pA and 0.180 V (tip positive), respectively.

adsorbed molecules is not easily controlled. As a consequence, tip-sample separation might be different for the two mutants and they may be subjected to different pressures by the tip, with possible effects on their conductivity [50,51].

3.2. AFM measurements

To gain deeper insight into the protein morphology, especially their height (which is not recovered in STM) and their orientation with respect to the gold substrate, we performed a systematic analysis by tapping mode atomic force microscopy (TMAFM). In this configuration lateral forces exerted on the proteins by the scanning tip are significantly reduced in comparison to contact mode, thus minimizing both damaging and indentation of the sample by the tip. All TMAFM images have been recorded in fluid conditions to eliminate capillary force and minimize height anomalies. These are often present in AFM images recorded in air and are caused by differences in adhesion at the sample surfaces as result of the inhomogeneous thickness of the adsorbed water layer [52].

Several TMAFM images were recorded from different zones of the adsorbed gold substrates under buffer solution. Since the isoelectric point

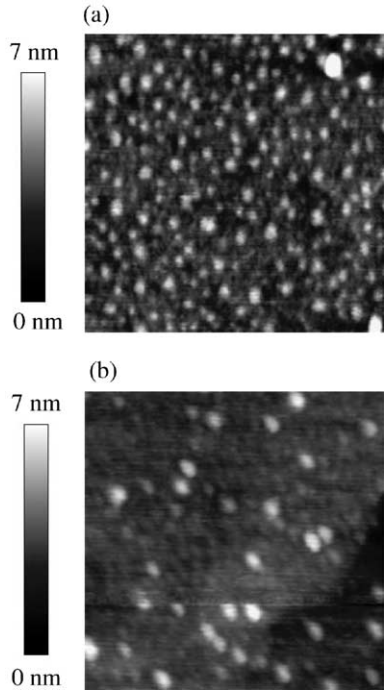

Fig. 9. Topographic images of PCSS (a) and PCSH (b) molecules adsorbed onto Au(1 1 1) as measured by tapping mode AFM in buffer solution. Scan area: 350×350 nm^2.

for silicon nitride tips has a value close to 6 [53], we chose a buffer solution with such pH value with further minimization of tip-sample interactions. Fig. 9 shows representative topographs of molecules of PCSS (a) and PCSH (b) adsorbed onto Au(1 1 1). Both mutants appear homogeneously distributed over the substrate and strongly bound to gold, as evidenced by high quality images even after repetitive scans. Representative high-resolution images are shown in Fig. 10(a) and (b) for PCSS and PCSH respectively. Individual molecules are well distinguishable above the substrate, which makes these samples suitable for statistical analysis of molecule height distribution with a vertical resolution of 0.1 nm. Minor information can be obtained about lateral dimensions of the proteins. In fact, the relatively large size of the tip and its geometry induces broadening effects in the biomolecule images so that lateral dimensions should be evaluated by deconvolution of the image with the tip shape [54].

The vertical dimension of the PC mutants was estimated from individual cross section analysis, as shown in Fig. 11 for PCSS molecules adsorbed onto gold. Data taken for hundreds of molecules are represented in the histograms of Fig. 12. The data for PCSS molecules have a mean value equal to 2.4 nm and a variance of 0.3 nm, whereas for PCSH the mean height is 1.9 nm with a variance of 0.4 nm. Comparing such dimensions with the crystallographic data we observe that for PCSS the data are centred at a value close to that expected for the protein anchored via the disulphide bridge ($h \sim 3$ nm), whereas the vertical dimension of PCSH above the gold substrate slightly differs from this value. To evaluate if standard deviations of the

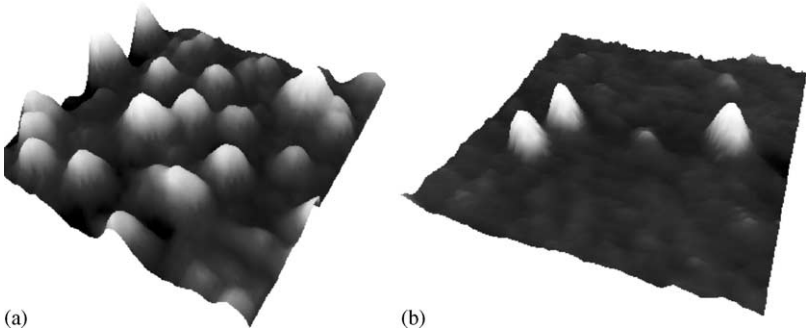

Fig. 10. High resolution images of PCSS (a) and PCSH (b) molecules adsorbed onto Au(1 1 1), recorded in buffer solution by TMAFM. Scan area: 145×145 nm^2 (a) and 140×140 nm^2 (b). Vertical range: 7 nm.

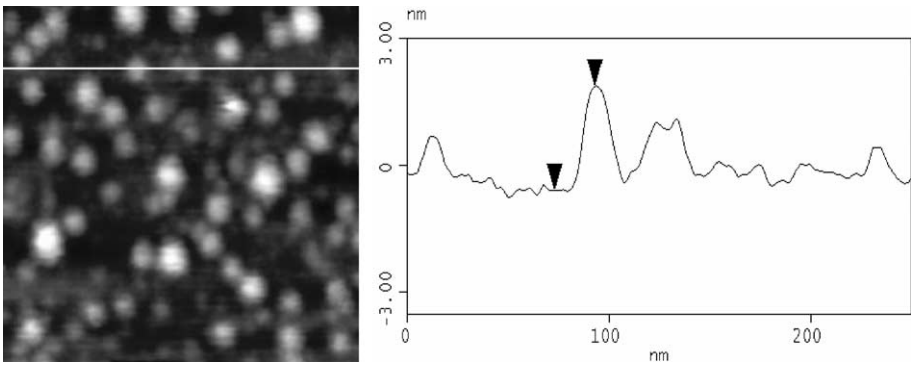

Fig. 11. TMAFM image of PCSS molecules adsorbed onto Au(1 1 1) recorded in buffer solution, with representative cross section profile. Scan area: 250×250 nm^2.

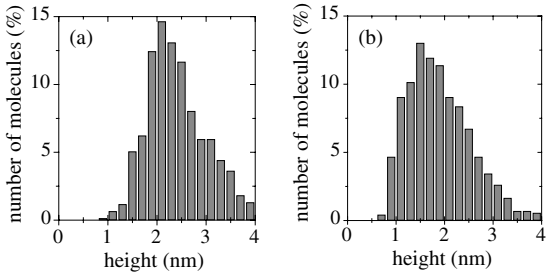

Fig. 12. Statistical analysis of the PCSS (a) and PCSH (b) molecular height above the Au(1 1 1) substrate, as measured by TMAFM under buffer solution. The vertical dimension of the proteins was estimated from individual cross section analysis of 772 different molecules for PCSS and 730 for PCSH. The height mean value is 2.3 nm for PCSS with a variance of 0.3 nm whereas for PCSH the mean height is 1.9 nm and the variance is 0.4 nm.

two sets of data are significantly different, the *F*-test has been executed which indicates that the standard deviation for the PCSH height distribution is higher than that for PCSS data with a confidence level of 95%. This result suggests that the disulphide bridge provides a stricter immobilisation and a more homogeneous orientation of PCSS molecules onto gold compared to PCSH, where the single thiol, external to the main structure of the protein, seems to allow protein to undergo reorientation. Moreover, a recent molecular dynamics simulation of PCSS adsorbed onto gold has pointed out a larger variability in both azimuth and polar angles of the copper-sulphur axis with respect to the gold surface when anchoring the protein by a single bond than when anchoring via the disulphide bridge [55]. As a consequence, a higher flexibility of molecules covalently bound to gold through one sulphur atom is expected than with binding via two covalent bonds. This behaviour is likely to find a correspondence with the distribution of protein heights above the substrate, which is expected to be broader for higher flexibility, consistently with our AFM data for PCSH molecules.

4. Conclusions

We have presented a SPM analysis of poplar plastocyanin mutants adsorbed onto gold via a disulphide bridge (PCSS) or a single thiol (PCSH). In particular, combined STM and TMAFM experiments have provided an extensive characterization at the single molecule level of a metalloprotein self assembled on Au(1 1 1) substrates.

Concerning topography, STM imaging does not reveal substantial differences in the lateral dimensions of the two mutants, which well agree with crystallographic values. Molecular height above the substrate has been evaluated by TMAFM experiments. The PCSS vertical dimension is consistent with the expected value for anchoring via the disulphide bridge, whereas for PCSH a slightly lower value is found. The narrower height distribution for PCSS compared to PCSH seems to indicate a more homogeneous orientation of molecules anchored to gold by the disulphide bridge than when anchored via a single thiol; the latter binding is likely to provide more motional freedom of the molecules above the substrate.

In electrochemical STM we found a reversibility of image contrast variation for PCSS, upon tuning the substrate potential close to and far from the midpoint potential. Under similar experimental conditions a different behaviour for PCSH molecules was observed, the STM image contrast being substantially unaffected. These findings are consistent with a tunneling mechanism mediated by the PCSS copper site, whereas no evidence of direct involvement of the PCSH redox site was detected. Correspondingly, STS experiments provide an asymmetric I–V relation for PCSS and symmetric I–V curves for PCSH. However, both mutants are well coupled to the electrode, with efficient conduction through the molecule towards the electrode, as may be expected for a covalent link to gold.

Alternative experimental techniques such as conductive AFM, which accounts for tip-sample interaction [56], may be proposed to study electronic properties of biomolecules. This method, already applied in the case of organic molecules [57], would allow to sense current and applied force simultaneously reducing tip-sample interactions.

Acknowledgements

This work has been partially supported by a PRIN MURST project and by the EC Project SAMBA (V Frame FET). Thanks are due to Dr. G. Costantini for help in generating Fig. 1 and to Prof. A. Rita Bizzarri and Dr. D. Alliata for discussions.

References

[1] C. Joachim, J.K. Gimzewski, A. Aviram, Nature 408 (2000) 541.
[2] I. Willner, B. Willner, Trends Biotech. 19 (2001) 222.
[3] H.C. Freeman, J.M. Guss, in: A. Messerschmidt, R. Huber, K. Wieghardt, T. Poulos (Eds.), Handbook of Metalloproteins, Wiley, 2001.
[4] K. Sigfridsson, M. Ejdeback, M. Sundahl, Ö. Hasson, Arch. Biochem. Biophys. 351 (1998) 197.
[5] W. Haehnel, T. Jansen, K. Gause, R.B. Klösgen, B. Stahl, D. Michl, B. Huvermann, M. Karas, R.G. Herrmann, EMBO J. 13 (1994) 1028.
[6] A. Ulman, Chem. Rev. 96 (1996) 1533.
[7] R.G. Nuzzo, B.R. Zegarski, L.H. Dubois, J. Am. Chem. Soc. 109 (1987) 733.
[8] H. Grönbeck, A. Curioni, W. Andreoni, J. Am. Chem. Soc. 122 (2000) 3839.
[9] E.P. Friis, J.E.T. Andersen, Y.I. Kharkats, A.M. Kuznestov, R.J. Nichols, J.-D. Zhang, J. Ulstrup, Proc. Nat. Acad. Sci. USA 96 (1999) 1379.
[10] Q. Chi, J. Zhang, J.U. Nielsen, E.P. Friis, I. Chorkendorff, G.W. Canters, J.E.T. Andersen, J. Ulstrup, J. Am. Chem. Soc. 122 (2000) 4047.
[11] J.J. Davis, H.A.O. Hill, A.M. Bond, Coord. Chem. Rev. 200–202 (2000) 411.
[12] I. Willner, E. Katz, Angew. Chem., Int. Ed. Engl. 39 (2000) 1180.
[13] P. Facci, D. Alliata, S. Cannistraro, Ultramicroscopy 89 (2001) 291.
[14] M.R. Redinbo, T.O. Yeates, S. Merchant, J. Bioenerg. Biomemb. 26 (1994) 49.
[15] B.A. Ivarsson, P.O. Hegg, I. Lundstrom, U. Jonsson, J. Colloid Interface Sci. 13 (1985) 169.
[16] M. Mrksich, G.B. Sigal, G.M. Whitesides, Langmuir 11 (1995) 4383.
[17] D. Kowalczyk, S. Slomkowski, J. Bioact. Compat. Polym. 9 (1994) 282.
[18] J.R. Lu, T.J. Su, P.N. Thirtle, R.K. Thomas, A.R. Rennie, R. Cubitt, Colloid Interface Sci. 206 (1998) 212.
[19] J.J. Davis, H.A.O. Hill, Chem. Commun. (2002) 393.
[20] S. Scheuring, D. Fotiadis, C. Möller, S.A. Müller, A. Engel, D.J. Müller, Single Molecules 2 (2001) 59.
[21] T.H. Bayburt, S.G. Sligar, Proc. Natl. Acad. Sci. 99 (2002) 6725.
[22] W. Han, E.N. Durantini, T.A. Moore, A.L. Moore, D. Gust, P. Rez, G. Leatherman, G.R. Seely, N. Tao, S.M. Lindsay, J. Phys. Chem. B 101 (1997) 10719, and references therein.
[23] G.B. Khomutov, L.V. Belovolova, S.P. Gubin, V.V. Khanin, A.Yu. Obydenov, A.N. Sergeev-Cherenkov, E.S. Soldatov, A.S. Trifonov, Bioelectrochemistry 55 (2002) 177.
[24] Gang-Yu Liu, Nabil A. Amro, Proc. Nat. Acad. Sci. 99 (2002) 5165.
[25] M. Bergkvist, J. Carlsson, S. Oscarsson, J. Phys. Chem. B 105 (2001) 2062.
[26] L. Andolfi, S. Cannistraro, G.W. Canters, P. Facci, A.G. Ficca, I.M.C. van Amsterdam, M.Ph. Verbeet, Arch. Biochem. Biophys. 399 (2002) 81.
[27] J.A. Ybe, M.H. Hecht, Protein Express Purif. 5 (1994) 317.
[28] B.H. Johnson, M.H. Hecht, Biotechnology 12 (1994) 1357.
[29] M. Milani, L. Andolfi, S. Cannistraro, M.Ph. Verbeet, M. Bolognesi, Acta Cryst. D 57 (2001) 1735.
[30] L. Andolfi, D. Bruce, S. Cannistraro, G.W. Canters, J.J. Davis, H.A.O. Hill, J. Crozier, M.Ph. Verbeet, C.W. Wrathmell, J. Electroanal. Chem., submitted for publication.
[31] J.J. Davis, C.M. Halliwell, H.A.O. Hill, G.W. Canters, M.C. van Amsterdam, M.Ph. Verbeet, New J. Chem. (1998) 1119.
[32] E.P. Friis, J.E.T. Andersen, L.L. Madsen, P. Møller, J. Ulstrup, J. Electroanal. Chem. 431 (1997) 35.
[33] J.J. Davis, D. Djuricic, K.K.W. Lo, E.N.K. Wallace, L.L. Wong, H.A.O. Hill, Faraday Discuss. 116 (2000) 15.
[34] S.L. Tang, A.J. McGhie, Langmuir 12 (1996) 1088.
[35] A. Bertazzon, B.M. Conti-Tronconi, M.A. Raftery, Proc. Nat. Acad. Sci. USA 89 (1992) 9632.
[36] M. Heim, R. Steigerwald, R. Guckenberger, J. Struct. Biol. 119 (1997) 212.
[37] W. Schmickler, J. Electroanal. Chem. 296 (1990) 283.
[38] A.M. Kuznetsov, J. Ulstrup, J. Phys. Chem. A 104 (2000) 11531.
[39] J. Zhang, Q. Chi, A.M. Kuznetsov, A.G. Hansen, H. Wackerbarth, H.E.M. Christensen, J.E.T. Andersen, J. Ulstrup, J. Phys. Chem. B 106 (2002) 1131.
[40] A.I. Onipko, K.-F. Berggren, Yu.O. Klymenko, L.I. Malysheva, J.J.W.M. Rosink, L.J. Geerlins, E. van der Drift, S. Radelaar, Phys. Rev. B 61 (2000) 11118.
[41] U. Mazur, K.W. Hipps, J. Phys. Chem. B 103 (1999) 9721.
[42] L. Scudiero, D.E. Barlow, U. Mazur, K.W. Hipps, J. Am. Chem. Soc. 123 (2001) 4073.
[43] K.W. Hipps, D.E. Barlow, U. Mazur, J. Phys. Chem. B 104 (2000) 2444.
[44] A. Aviram, M.A. Ratner, Chem. Phys. Lett. 29 (1974) 277.
[45] R.M. Metzger, Acc. Chem. Res. 32 (1999) 95.
[46] M.L. Chabinyc, X. Chen, R.E. Holmlin, H. Jacobs, H. Skulason, C.D. Frisbie, V. Mujica, M.A. Ratner, M.A. Rampi, G.M. Whitesides, J. Am. Chem. Soc. 124 (2002) 11730.
[47] A. Troisi, M. Ratner, J. Am. Chem. Soc. 124 (2002) 14528.
[48] A.J. Ikushima, T. Kanno, S. Yoshida, A. Maeda, Thin Solid Films 273 (1996) 35.

[49] L. Andolfi, S. Cannistraro, G.W. Canters, J.J. Davis, M.Ph. Verbeet, H.A.O. Hill, in preparation.
[50] U. Dürig, O. Züger, B. Michel, L. Häusslinh, H. Ringsdorf, Phys. Rev. B 48 (1993) 1711.
[51] K.W. Hipps, Science 294 (2001) 536.
[52] S. John, T. Van Noort, K.O. Van der Werf, B.G. De Grooth, N.F. Van Hulst, J. Greve, Ultramicroscopy 69 (1997) 117.
[53] X.Y. Lin, F. Creuzet, H. Arribart, J. Phys. Chem. 97 (1993) 7272.
[54] P. Markiewicz, M.C. Goh, J. Vac. Sci. Technol. B 13 (1995) 1115.
[55] G. Costantini, A.R. Bizzarri, S. Cannistraro, J. Phys. Chem. B, submitted for publication.
[56] G. Leatherman, E.N. Durantini, D. Gust, T.A. Moore, A.L. Moore, S. Stone, Z. Zhou, P. Rez, Y.Z. Liu, S.M. Lindsay, J. Phys. Chem. B 103 (1999) 4006.
[57] X.C. Cui, A. Primak, X. Zarate, J. Tomfohr, O.F. Sankey, A.L. Moore, T.A. Moore, D. Gust, G. Harris, S.M. Lindsay, Science 294 (2001) 571.